energies

Article

Coupled Effects of Lorentz Force, Radiation, and Dissipation on the Dynamics of a Hybrid Nanofluid over an Exponential Stretching Sheet

Muhammad Zahid [1], Abdul Basit [1,*], Tariq Ullah [1], Bagh Ali [2] and Grzegorz Liśkiewicz [1]

[1] Institute of Turbomachinery, Lodz University of Technology, Wolczanska 219/223, 90-924 Lodz, Poland; muhammad.zahid@dokt.p.lodz.pl (M.Z.); tariq.ullah@dokt.p.lodz.pl (T.U.); grzegorz.liskiewicz@p.lodz.pl (G.L.)

[2] School of Mechanical Engineering and Automation, Harbin Institute of Technology, Shenzhen 518055, China; bagh@hit.edu.cn

* Correspondence: abdul.basit@dokt.p.lodz.pl

Abstract: The flow and heat transfer induced by an exponentially shrinking sheet with hybrid nanoparticles are investigated comprehensively in this paper. Nanoparticles are considered due to their unusual characteristics such as extraordinary thermal conductivity, which is significant in advanced nanotechnology, heat exchangers, material sciences, and electronics. The main objective of this research is to enhance heat transportation. The flow model is first transformed and simplified to a system of ordinary differential equations utilizing non-dimensional quantities and similarity functions. Then, the desired system is solved with the help of the Runge–Kutta numerical method and the shooting technique in MATLAB script. The results show that a stronger porosity parameter raises the temperature while diminishing the velocity. Additionally, they emphasize that augmentations in the magnetic parameter, Eckert number, radiation parameter, and the volume fractions of titanium dioxide and silver nanoparticles are all proportional to the temperature profile.

Keywords: hybrid nanofluids; viscous dissipation; radiation; exponential stretching sheet

Citation: Zahid, M.; Basit, A.; Ullah, T.; Ali, B.; Liśkiewicz, G. Coupled Effects of Lorentz Force, Radiation, and Dissipation on the Dynamics of a Hybrid Nanofluid over an Exponential Stretching Sheet. *Energies* **2023**, *16*, 7452. https://doi.org/10.3390/en16217452

Academic Editors: Frede Blaabjerg and Gianpiero Colangelo

Received: 30 August 2023
Revised: 22 September 2023
Accepted: 3 November 2023
Published: 5 November 2023

1. Introduction

Nanofluids are specific types of fluids that have nanoparticles scattered throughout a conventional fluid, usually liquids such as water, engine oil, or kerosene. These conventional heat transfer fluids possess limited heat transfer capabilities due to their relatively low thermal conductivity. This limitation hinders their effectiveness in enhancing the performance and compactness of various engineering electronic devices. As a consequence, there is a great need to develop heat transfer fluids with considerably increased conductive qualities as a means of improving their thermal properties. The presence of nanoparticles in fluids can substantially augment both the effective thermal conductivity and viscosity of the base fluid, leading to a significant enhancement in its heat transfer capabilities. Early research looked into the ways in which nanofluids can improve heat transfer. Choi et al. [1] presented experimental data showing enhanced thermal performance in comparison to base fluid when analyzing the effects of nanoparticle dispersion. This study contributed to the understanding of nanofluid behavior and its potential applications. Khan and Pop [2] were the first to analyze the development of the steady boundary layer flow, heat transfer, and nanoparticle fraction over a stretching surface in a nanofluid. Hayat et al. [3] studied the impact of silver and copper nanoparticles on the entropy of a viscous fluid produced by a rotating disk, finding that the surface drag force and Nusselt number both increase as the volume fraction of the nanoparticles is enhanced. Hsiao [4] presented heat and mass transfer in a hydromagnetic flow featuring magnetic and viscous dissipation effects with micropolar nanofluids near a stretching sheet. It was assumed that magnetic field and

Joule heating were induced. References to nanofluids can be found by Akbar et al. [5], Mustafa et al. [6], Ibrahim et al. [7], Mathews and Hymavathi [8], and Javed et al. [9], all of which have demonstrated the importance of the stagnation fluid flow.

In recent years, there has been growing interest in the innovative concept of enhancing heat transfer within boundary layer flow problems through the application of hybrid nanofluids. It is believed that these characteristics can significantly improve heat transfer rates in comparison to regular nanofluids, primarily due to their synergistic effects [10]. Devi and Devi [11] conducted a study focusing on the flow past a permeable stretched surface while considering the influence of hydromagnetic effects. They utilized a hybrid nanofluid consisting of different nanoparticles suspended in water, and introduced a novel thermophysical model specific to hybrid nanofluids. Recently, Khashi'ie et al. [12] investigated the flow of a hybrid nanofluid over a shrinking disc, observing that the heat transfer rate decreased as the hybrid nanoparticles concentration increased. This phenomenon was attributed to the greater suction force applied to the shrinking sheet. Various researchers have used the thermophysical approach to examine the influence of physical factors on hybrid nanofluid flows, including Leong et al. [13], Gul and Saeed [14], Basit et al. [15], Mahabaleshwar et al. [16], Kayalvizhi and Kumar [17], and Waqas et al. [18].

The flow over a stretching surface plays an important role in many engineering processes, including extrusion, metal spinning, hot rolling, wire drawing, crystal growing, production of glass fiber, production of plastic and rubber sheets, cooling of filaments, and more. In the historical context of fluid dynamics, the investigation of a steady two-dimensional flow over a linearly stretched surface can be attributed to the pioneering research conducted by Crane [19]. Magyari and Keller [20] were the first to propose the use of an exponentially stretched surface to investigate the distribution of the wall temperature and its effect on the flow and heat transfer characteristics. They found that for any fixed Prandtl number, raising the temperature distribution parameter reduces the thickness of the thermal boundary layer. Hayat et al. [21] worked on the melting heat transfer and radiation effects within the stagnation point flow of a carbon–water nanofluid. Their findings revealed that higher values of the melting parameter in combination with smaller nanoparticle volume fractions led to a decrease in the skin friction coefficient. Mabood et al. [22] developed an analytical solution for MHD boundary layer flow over an exponentially stretching sheet while considering thermal radiation. They found that the magnetic and radiation parameters significantly influence the flow characteristics, resulting in increased temperature within the thermal boundary layer and friction. Recently, Zaib et al. [23] studied the impact of nanoparticles on flow and heat transfer over an exponentially shrinking sheet, discovering that the thermal boundary layer thickness is enhanced as the nanoparticle volume fraction increases due to the shrinking sheet. Following this innovative study, flow field over extending surfaces has received considerable attention, and a great deal has been written on it. Examples include Aziz [24], Dessie and Kishan [25], Cortell et al. [26], Rafique et al. [27], Alharbi et al. [28], Yirga et al. [29], and Hayat et al. [30].

In our study, we consider the coupling of the Lorentz force, radiation, and dissipation effects together, which is essential in order to provide a comprehensive understanding of nanofluid behavior. These interactions are all interconnected and collectively influence the heat transfer and flow characteristics of nanofluids, especially in scenarios involving magnetic fields and elevated temperatures. Investigating them together can provide a comprehensive and precise representation of nanofluid phenomena [31].

Although many outcomes have been reported in the literature, they have not been properly analyzed as a whole. Therefore, the objective of the present study is to investigate the effects of hybrid nanoparticles on fluid flow and heat transfer induced by an exponentially stretching sheet. A model of titanium dioxide (TiO_2) and silver (Ag) nanoparticles with water (H_2O) as the base fluid is assumed. This approach provides an innovative perspective on modeling the various forces involved in heat transfer for such hybrid nanofluids. For validation purposes, the numerical outcomes of this study are compared with previously published data. The current research has applications in metal spinning, drawing of plastic films, glass blowing, crystal growth, and filament cooling [32]. The objective of this study is to provide numerical answers to the following research questions:

- What impact do the relevant parameters have on the flow profiles?
- What changes occur in the heat transfer rate due to the hybrid nanofluid?
- What are the impacts of the critical parameters on the physical quantities?

2. Mathematical Formulation

A time-independent 2-dimensional TiO_2-Ag/H_2O hybrid nanofluid flow is examined via an exponentially stretching sheet. The x-axis lies parallel to the stretching surface and the y-axis is perpendicular to the surface, as shown in Figure 1. The sheet accelerates in the x-direction $(x \geq 0)$ at an exponential rate $\bar{U}_w = c_0 e^{\frac{x}{l}}$, and its velocity profile is $\bar{v}_w = v_0 e^{\frac{x}{2l}}$. We denote the reference length as l, while c_0 and v_0 are both positive constants. The sheet is kept at an exponentially changing temperature $\bar{T}_w = \bar{T}_\infty + \bar{T}_0 e^{\frac{x}{2l}}$, where $\bar{T}_0$ is the reference value and $\bar{T}_\infty$ is the ambient value. The variable magnetic field is $\bar{B}x = \bar{B}_0 e^{\frac{x}{2l}}$, where $\bar{B}_0$ represents the uniform magnetic strength normally applied to the flow region. The effects of porosity $\bar{K}x = \bar{K}_0 e^{\frac{-x}{l}}$ and changing heat source $\bar{Q}x = \bar{Q}_0 e^{\frac{x}{l}}$ are considered as well.

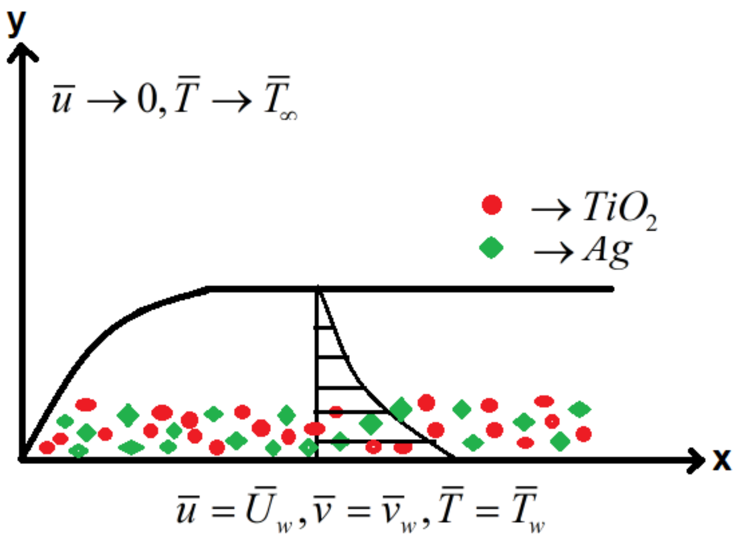

Figure 1. Geometry of the problem.

Under the above conditions, the governing equations are as follows [33,34].
Continuity equation:

$$\bar{u}_x + \bar{v}_y = 0. \tag{1}$$

Momentum equation:

$$\bar{u}\bar{u_x} + \bar{v}\bar{u_y} = \left(\frac{\mu_{hnf}}{\rho_{hnf}}\right)\bar{u_{yy}} - \frac{\sigma_{hnf}}{\rho_{hnf}}\bar{B}^2(x)\bar{u} + \left(\frac{\mu_{hnf}}{\rho_{hnf}}\right)\frac{\bar{u}}{\bar{K}}. \tag{2}$$

Energy equation:

$$\bar{u}\bar{T_x} + \bar{v}\bar{T_y} = \alpha_{hnf}\bar{T_{yy}} - \frac{1}{(\rho C_p)_{hnf}}\frac{\partial q_r}{\partial y} + \frac{\bar{Q}}{(\rho C_p)_{hnf}}(\bar{T} - \bar{T}_\infty) + \frac{\mu_{hnf}}{(\rho C_p)_{hnf}}\bar{u_y}^2. \tag{3}$$

Equation (1) describes the mass conservation for an incompressible flow, while Equations (2) and (3) introduce the rate of convection change on the left-hand side. In Equation (2), the right-hand side consists of three distinct terms; the first represents viscous effects, the second signifies body forces, particularly magnetic effects, and the third relates to thermal conductivity. In Equation (3), the right-hand side can be categorized similarly; the first term deals with thermal diffusion, the second involves flux gradients, the third encompasses heat generation and temperature differences, and the fourth accounts for viscous dissipation.

The boundary conditions are provided by

$$\begin{aligned} &\bar{u} = \bar{U}_w,\ \bar{v} = \bar{v}_w,\ \bar{T} = \bar{T}_w, at\ y \to 0, \\ &\bar{u} \to 0,\ \bar{T} \to \bar{T}_\infty, as\ y \to \infty. \end{aligned} \tag{4}$$

For the Rosseland approximation q_r [35], Equation (3) can be written as follows:

$$\bar{u}\bar{T}_x + \bar{v}\bar{T}_y = \bar{T}_{yy}\left(\alpha_{hnf} + \frac{16\sigma^* T_\infty^3}{(\rho C_p)_{hnf} 3k_1}\right) + \frac{\bar{Q}}{(\rho C_p)_{hnf}}(\bar{T} - \bar{T}_\infty) + \frac{\mu_{hnf}}{(\rho C_p)_{hnf}}\bar{u}_y{}^2. \tag{5}$$

Next, the similarity transformation [36,37] is introduced:

$$\eta = y\sqrt{\frac{a_0}{2\nu\ell}}e^{\frac{x}{2\ell}},\ \bar{u} = c_0 e^{\frac{x}{\ell}} f'(\eta),\ \bar{v} = -\sqrt{\frac{c_0\nu}{2\ell}}e^{\frac{x}{2\ell}}[f(\eta) + \eta f'(\eta)],\ \bar{T} = \bar{T}_\infty + \bar{T}_0 e^{\frac{x}{2\ell}}\theta(\eta). \tag{6}$$

In view of the above appropriate relations, Equation (1) is satisfied identically; Equations (2) and (3) respectively become [33,34]

$$f''' - a_1 a_3 M f' - 2a_1 a_2 f'^2 - K_p f' + a_1 a_2 f f'' = 0, \tag{7}$$

$$a_1\left(a_5 + \frac{4}{3}R_d\right)\theta'' + a_1 a_4 Pr f\theta' - a_1 Pr(a_4 f' - \beta)\theta + PrEc f''^2 = 0, \tag{8}$$

and the boundary conditions can be transformed into

$$f'(0) = 1,\ f(0) = s,\ \theta(0) = 1,\ at\ \eta = 0, \tag{9}$$

$$f'(\infty) \to 0,\ \theta(\infty) \to 0.\ as\ \eta \to \infty. \tag{10}$$

The aforementioned system was solved numerically by the Runge-Kutta method with the shooting technique in MATLAB R2023a, Mathworks, Lodz, Poland. The availability of the chosen numerical method was demonstrated by the precise agreement of the surface temperature gradient with previously published results, shown in the remarkable agreement appearing in Table 1.

The associated non-dimensional parameters are provided by

$$M = \frac{2\sigma_f B_0^2 \ell}{(Cp)_f},\ Pr = \frac{\mu_f (Cp)_f}{k_f},\ Ec = \frac{\bar{U}_w^2}{(Cp)_f(\bar{T}_w - \bar{T}_\infty)}, R_d = \frac{4\sigma^* \bar{T}_\infty^3}{k^* k_f}, K_p = \frac{2l\nu_f}{c_0 K_0},\ \beta = \frac{2lQ_0}{c_0(\rho Cp)_f},\ s = -v_0\sqrt{\frac{2l}{\nu_f c_0}}.$$

The wall shear stress and thermal flux are respectively provided by the relations

$$Cf_x - \frac{\mu_{hnf}}{\rho_f \bar{U}_w^2}\left(\frac{\partial \bar{u}}{\partial y}\right)_{y=0} = 0, \tag{11}$$

$$Nu_x + \frac{2l}{k_f(\bar{T}_w - \bar{T}_\infty)}\left(-k_{hnf}\left(\frac{\partial \bar{T}}{\partial y}\right)_{y=0} + (q_r)_{y=0}\right) = 0. \tag{12}$$

The skin friction Cf_x and Nusselt number Nu_x in dimensionless form are

$$Cf_x Re_x^{\frac{1}{2}} = \left(\frac{f''(0)}{a_1}\right), Nu_x Re_x^{\frac{-1}{2}} = -\left(a_4 + \frac{4}{3}R_d\right)\theta'(0). \tag{13}$$

The thermophysical properties of the base fluid and nanoparticles are shown in Table 2.

Table 1. Comparison of $-\theta'(0)$ with different values of R_d, M, and Pr.

R_d	M	Pr	Goud et al. [33]	Ishak et al. [36]	Bidin et al. [38]	Current Results
0.0	0	1.0	0.954784	0.9548	0.9547	0.9548106
		2.0	1.471462	1.4715	1.4714	1.4714540
		3.0	1.869073	1.8691	1.8691	1.8690688
		5.0	2.500111	2.5001		2.5001280
		10.0	3.660346	3.6604		3.6603693
	1.0	1.0	0.861097	0.8611		0.8615086
1.0	0.0		0.53117	0.5312	0	0.5313112
	1.0		0.450687	0.4505	0	0.4506955

Table 2. The hybrid nanofluid's efficient thermophysical models, as provided by [34].

Properties	Hybrid Nanofluid
Dynamic Viscosity	$\frac{\mu_{hnf}}{\mu_f} = \frac{1}{(1-\phi_1)^{2.5}(1-\phi_2)^{2.5}} = \frac{1}{a_1}$
Density	$\frac{\rho_{hnf}}{\rho_f} = (1-\phi_2)\left[1-\phi_1+\phi_1\left(\frac{\rho_{s1}}{\rho_f}\right)\right]+\phi_2\left(\frac{\rho_{s2}}{\rho_f}\right) = a_2$
Electrical Conductivity	$\frac{\sigma_{hnf}}{\sigma_f} = 1+\frac{3\left(\frac{\phi_1\sigma_1+\phi_2\sigma_2}{\sigma_f}-(\phi_1+\phi_2)\right)}{2+\left(\frac{\phi_1\sigma_1+\phi_2\sigma_2}{\sigma_f(\phi_1+\phi_2)}\right)-\left(\frac{\phi_1\sigma_1+\phi_2\sigma_2}{\sigma_f}-(\phi_1+\phi_2)\right)} = a_3$
Specific Heat	$\frac{(\rho Cp)_{hnf}}{(\rho Cp)_f} = (1-\phi_2)\left[1-\phi_1+\phi_1\left(\frac{(\rho Cp)_{s1}}{(\rho Cp)_f}\right)\right]+\phi_2\left(\frac{(\rho Cp)_{s2}}{(\rho Cp)_f}\right) = a_4$
Thermal Conductivity	$\frac{k_{hnf}}{k_f} = a_5$, where $\frac{k_{hnf}}{k_f} = \frac{k_{s2}+2k_{nf}-2\phi_2(k_{nf}-k_{s2})}{k_{s2}+2k_{nf}+2\phi_2(k_{nf}-k_{s2})}$ and $\frac{k_{nf}}{k_f} = \frac{k_{s1}+2k_f-2\phi_1(k_f-k_{s1})}{k_{s1}+2k_f+2\phi_1(k_f-k_{s1})}$

3. Implementation of the Method

The system of ODEs in Equations (7) and (8), subject to the boundary conditions in Equations (9) and (10), is solved numerically using the shooting method [39]. To convert Equations (7) and (8) into a system of first-order ODEs, we introduce the new variables $f = y_1$, $f' = y_2$, $f'' = y_3$, $\theta = y_4$, $\theta' = y_5$ to make up the following set of five first-order ordinary differential equations:

$$\begin{aligned}
y_1' &= y_2, \\
y_2' &= y_3, \\
y_3' &= y_2(a_1a_3M + kp + 2a_1a_2y_2) - a_1a_2y_1y_3, \\
y_4' &= y_5, \\
y_5' &= -\frac{(a_1a_4Pry_1y_5 + a_1Pr(\beta - a_4y_2)y_4 + PrEcy_3^2)}{a_1(a_4 + \frac{4R_d}{3})}.
\end{aligned}$$

The corresponding dimensionless boundary conditions are

$$\begin{aligned}
&y_1 = s,\ y_2 = 1, y_4 = 1,\ at\ \eta = 0, \\
&y_2 \to 0,\ y_4 \to 0,\ as\ \eta \to \infty.
\end{aligned}$$

To solve the above system of first-order ODEs using the shooting method, five initial conditions are required. To do this, we first guess two unknown initial conditions $y_3(0) = p$ and $y_5(0) = q$. Suitable guesses for two unknown missing conditions p and q are chosen such that the two known boundary conditions are approximately satisfied for $\eta \to \infty$. Newton's iterative scheme is applied to improve the accuracy of the missing initial conditions p and q until the desired approximation is met. Our computations were performed for the various emerging parameters and the appropriate bounded domain $[0, \eta_{\max}]$ instead of $[0, \infty)$, with the positive real number $\eta_{\max}$ chosen to ensure that no significant variations appear in the results for values greater than $\eta_{\max}$. The stopping criteria for the iterative process is

$$\max(|y_2(\eta_{\max}) - 0|, |y_4(\eta_{\max}) - 0|) < \zeta, \tag{14}$$

where ζ is a very small positive real number.

4. Validation of the Numerical Scheme

For all our computations, ξ was chosen as 10^{-7}. To further ensure the reliability and validity of the code, the results of $-\theta^{'}(0)$ were checked against the rising inputs of M, R_d, and Pr as reported by Goud et al. [33], Ishak et al. [36], and Bidin et al. [38], which were successfully reproduced as presented in Table 1. Furthermore, the Matlab-created RK computations showed a high rate of convergence. Thus, our numerical calculations are validated.

5. Results and Discussion

The system of ODEs in Equations (7) and (8) was solved numerically by implementing the Runge–Kutta method with the shooting technique in MATLAB. The basic discretization methods were the finite difference method (FDM), finite volume method (FVM), and finite element method (FEM). However, the computational costs and time required by these methods are much higher for calculating unknowns as compared to the Runge–Kutta method. The Runge–Kutta method with shooting technique is a powerful scheme for solving ODEs and finding the solutions of flow problems. The physical influence of suitable parameters on the velocity and temperature profiles is demonstrated in Figures 2–12.

The velocity profiles in Figure 2 demonstrate that the rate of transport decreases significantly when the magnetic parameter M leads to an increase in the Lorentz force. This indicates that the transverse magnetic field opposes transport, likely due to increased resistance caused by changes in the Lorentz force. However, the velocity gradient representing the surface shear stress increases with rising M. Therefore, M acts as a control parameter for the surface shear stress. Figure 3 depicts the variation of the velocity $f'(\eta)$ with η for several values of the porosity parameter K_p. This is explained physically by the fact that an increase in the K_p parameter reduces fluid velocity, as higher K_p values indicate a greater proportion of larger pores within the porous medium. This increased void space offers less resistance to fluid flow, allowing the fluid to move more slowly through the medium. The impact of the suction parameter s upon the velocity field can be seen in Figure 4. It can be observed that increasing the suction parameter s in a fluid flow leads to a significant decrease in velocity. This is consistent with the physical reality that when s increases, the stretched sheet that interrupts the flow momentum remains with the boundary layer of momentum, causing a decrease in the boundary layer thickness and a reduction in the velocity field.

Figure 5 shows the impact of the magnetic parameter M on the temperature profiles. From the profiles, it can be seen that an increase in M leads to the production of a Lorentz force that increases the friction between the fluid layers, in turn causing thicker thermal boundary layers that improve the temperature profile. The influence of the radiation parameter R_d on the temperature field $\theta(\eta)$ can be seen in Figure 6. Increasing the radiation parameter R_d leads to an increase in temperature, as higher R_d values indicate a greater contribution of radiative heat transfer, elevating the overall temperature within the system. Thus, radiative heat transfer becomes more significant, resulting in higher temperatures, especially near radiative heat sources. Figure 7 demonstrates the favorable effect of the Eckert number Ec on the temperature field, with an increase in the Eckert number Ec leading to an increase in temperature. Physically, higher values of Ec signify that kinetic energy dominates over thermal energy in the fluid flow, resulting in increased temperature. Figures 8 and 9 respectively show how the heat source β and porosity parameters K_p produce an internal heat source (which can be seen in [40,41]) that boosts the fluid temperature. Figure 10 visualizes the effect of the suction parameter s on the temperature field. It can be observed that increasing the suction parameter s leads to a decrease in temperature. Physically, suction removes fluid from the system, which can result in reduced temperatures, particularly near the suction point. Figures 11 and 12 respectively show the favorable influence of the volume fraction of Ag and TiO_2 nanoparticles on $\theta(\eta)$. Physically, this because the inclusion of Ag and TiO_2 nanoparticles increases particle collision and improves fluid thermal conductivity.

The effects of significant parameters on the skin friction coefficient and Nusselt number are presented in Tables 3 and 4, respectively. With modifications in the values of M, K_p, s, ϕ_1, and ϕ_2, the drag coefficient diminishes; see Table 3. These variables constrict the flow, which in turn reduces the drag coefficient. Because R_d enhances the surface heat flux, the thermal transportation rises with R_d, and conversely decreases with increased values of M, Ec, β, ϕ_1, and ϕ_2 (see Table 4). Table 5 shows the values of thermophysical features of water and used nanoparticles.

Table 3. Variation of $Cf_x Re_x^{\frac{1}{2}}$ with Pr = 6.2, R_d = 1, Ec = 0.3, and β = 0.1.

M	K_p	s	ϕ_1	ϕ_2	$Cf_x Re_x^{\frac{1}{2}}$
0.5	1.0	0.1	0.1	0.1	−3.2211
1.0	1.0	0.1	0.1	0.1	−3.3551
1.5	1.0	0.1	0.1	0.1	−3.4836
2.0	1.0	0.1	0.1	0.1	−3.6073
1.0	0.5	0.1	0.1	0.1	−3.1246
1.0	1.0	0.1	0.1	0.1	−3.3551
1.0	1.5	0.1	0.1	0.1	−3.5699
1.0	2.0	0.1	0.1	0.1	−3.7719
1.0	1.0	0.1	0.1	0.1	−3.3551
1.0	1.0	0.2	0.1	0.1	−3.4634
1.0	1.0	0.3	0.1	0.1	−3.5754
1.0	1.0	0.4	0.1	0.1	−3.6911
1.0	1.0	0.1	0.01	0.1	−2.5458
1.0	1.0	0.1	0.02	0.1	−2.6292
1.0	1.0	0.1	0.03	0.1	−2.7140
1.0	1.0	0.1	0.04	0.1	−2.8003
1.0	1.0	0.1	0.1	0.01	−2.8315
1.0	1.0	0.1	0.1	0.02	−2.8848
1.0	1.0	0.1	0.1	0.03	−2.9392
1.0	1.0	0.1	0.1	0.04	−2.9947

Table 4. Variation of $Nu_x Re_x^{\frac{-1}{2}}$ with Pr = 6.2, K_p = 1, and s = 0.1.

M	Ec	R_d	β	ϕ_1	ϕ_2	$Nu_x Re_x^{\frac{-1}{2}}$
0.5	0.3	1.0	0.1	0.1	0.1	1.3487
1.0	0.3	1.0	0.1	0.1	0.1	1.1466
1.5	0.3	1.0	0.1	0.1	0.1	0.9518
1.0	0.1	1.0	0.1	0.1	0.1	2.8107
1.0	0.2	1.0	0.1	0.1	0.1	1.9786
1.0	0.3	1.0	0.1	0.1	0.1	1.1466
1.0	0.3	0.5	0.1	0.1	0.1	0.9698
1.0	0.3	1.0	0.1	0.1	0.1	1.1466
1.0	0.3	1.5	0.1	0.1	0.1	1.2565
1.0	0.3	1.0	0.15	0.1	0.1	0.9012
1.0	0.3	1.0	0.20	0.1	0.1	0.5671
1.0	0.3	1.0	0.25	0.1	0.1	−1.1570

Table 4. *Cont.*

M	Ec	R_d	β	ϕ_1	ϕ_2	$Nu_x Re_x^{\frac{-1}{2}}$
1.0	0.3	1.0	0.1	0.01	0.1	1.8109
1.0	0.3	1.0	0.1	0.02	0.1	1.7405
1.0	0.3	1.0	0.1	0.03	0.1	1.6694
1.0	0.3	1.0	0.1	0.1	0.01	1.4423
1.0	0.3	1.0	0.1	0.1	0.02	1.4131
1.0	0.3	1.0	0.1	0.1	0.03	1.3831

Table 5. Thermophysical properties of water and used nanoparticles [15].

Properties	H_2O	Ag	TiO_2
ρ (kg/m^3)	997.1	10,500	4250
Cp (J/kgK)	4179	235	686.2
k (W/mK)	0.613	429	8.9538
σ (S/m)	5×10^{-2}	3.5×10^6	2.38×10^6

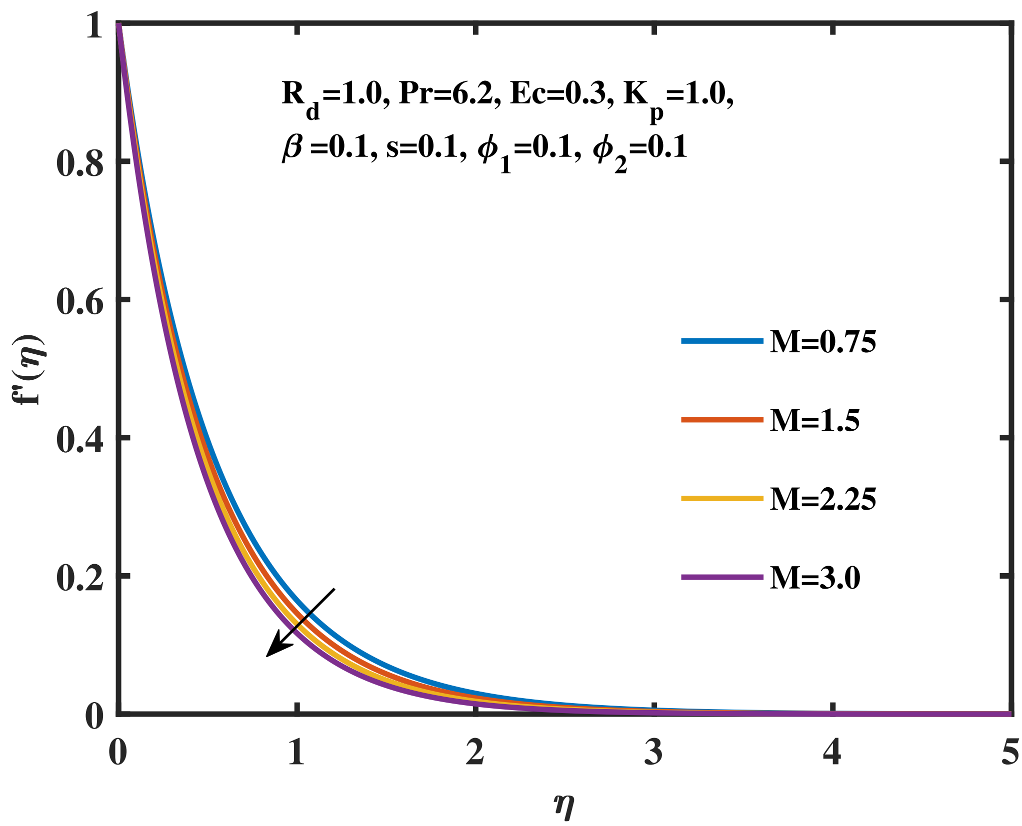

Figure 2. Variation of the velocity $f'(\eta)$ with η for several values of the magnetic parameter M.

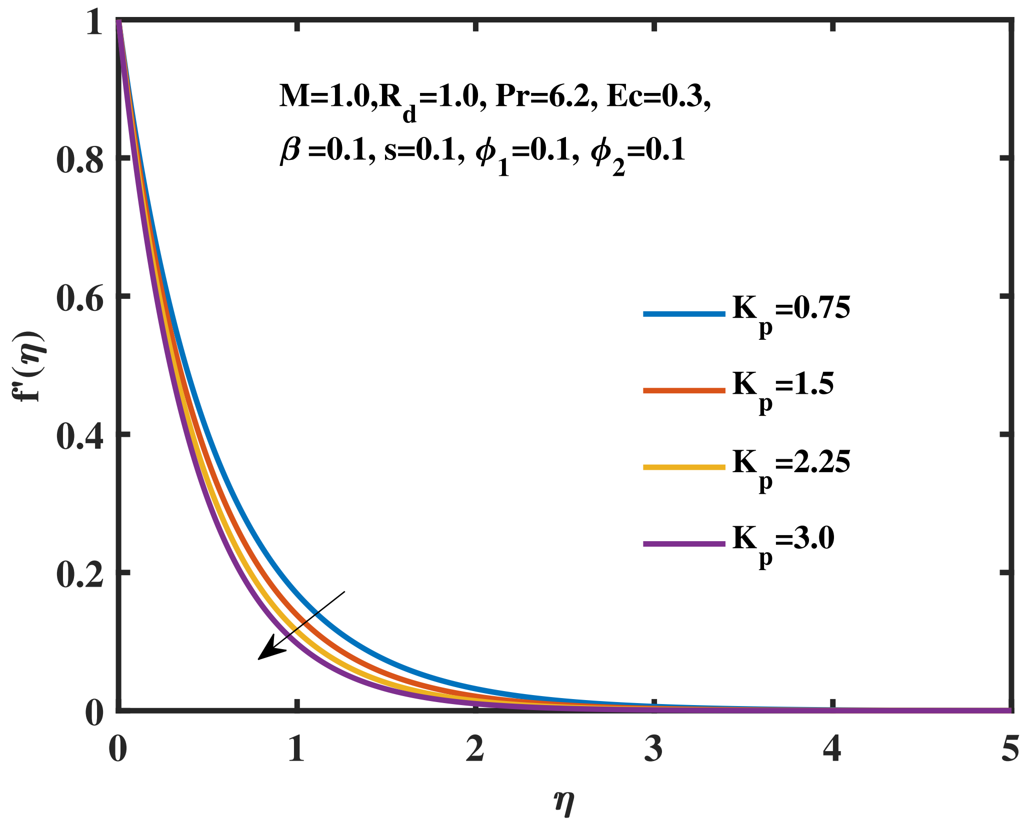

Figure 3. Variation of the velocity $f'(\eta)$ with η for several values of the porosity parameter K_p.

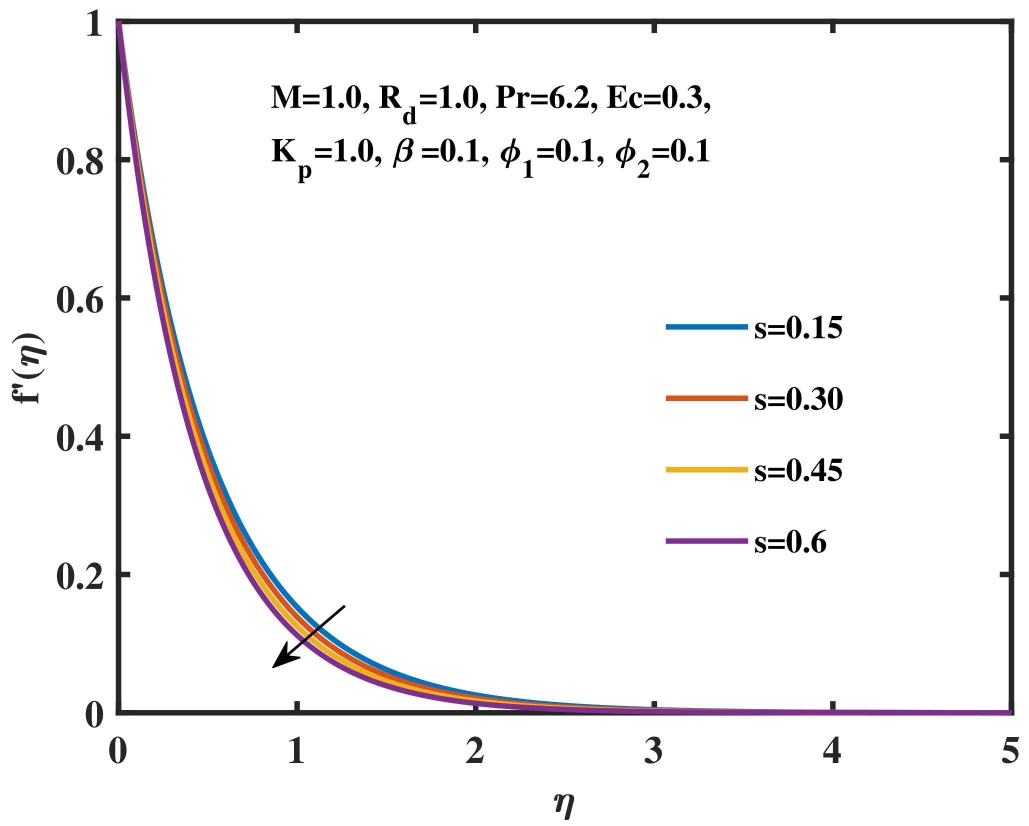

Figure 4. Variation of velocity $f'(\eta)$ with η for several values of the suction parameter s.

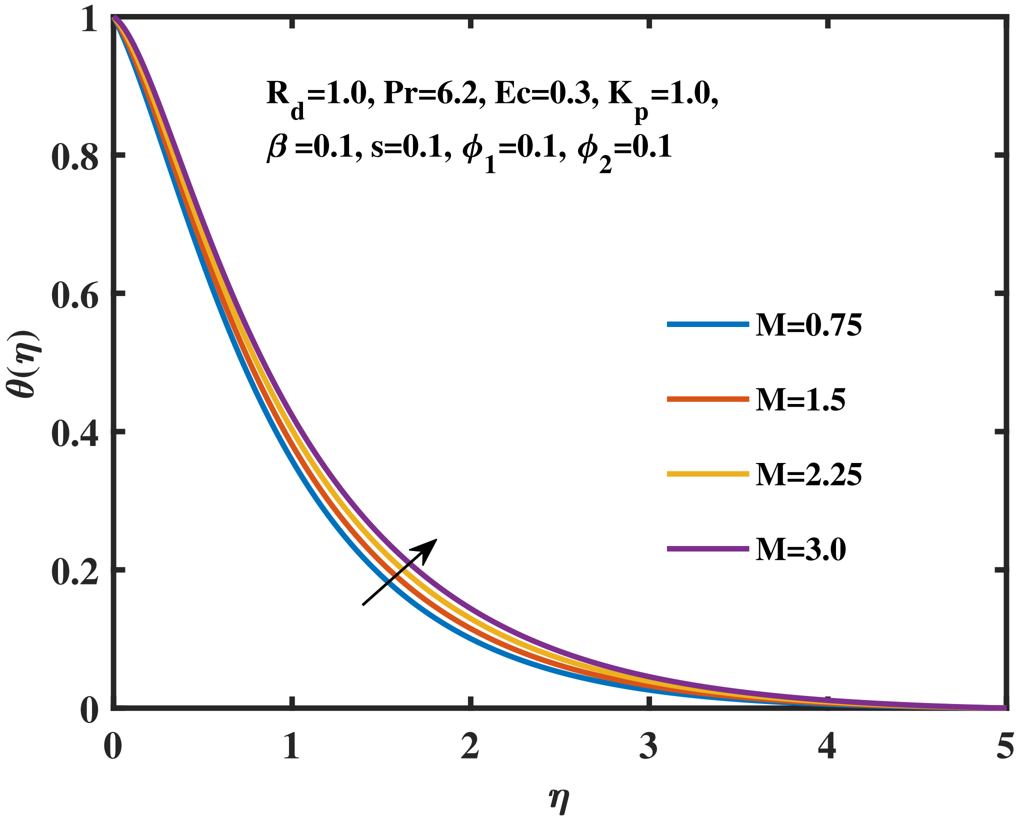

Figure 5. Variation of the temperature $\theta(\eta)$ with η for several values of magnetic parameter M.

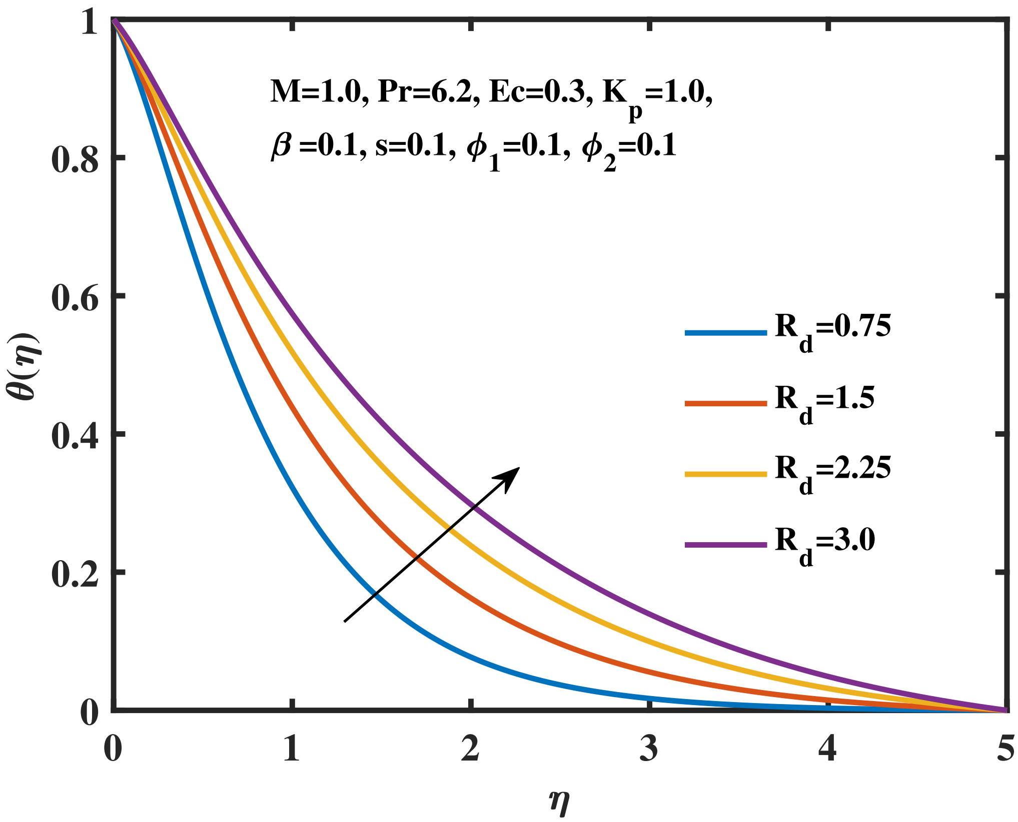

Figure 6. Variation of temperature $\theta(\eta)$ with η for several values of the radiation parameter R_d.

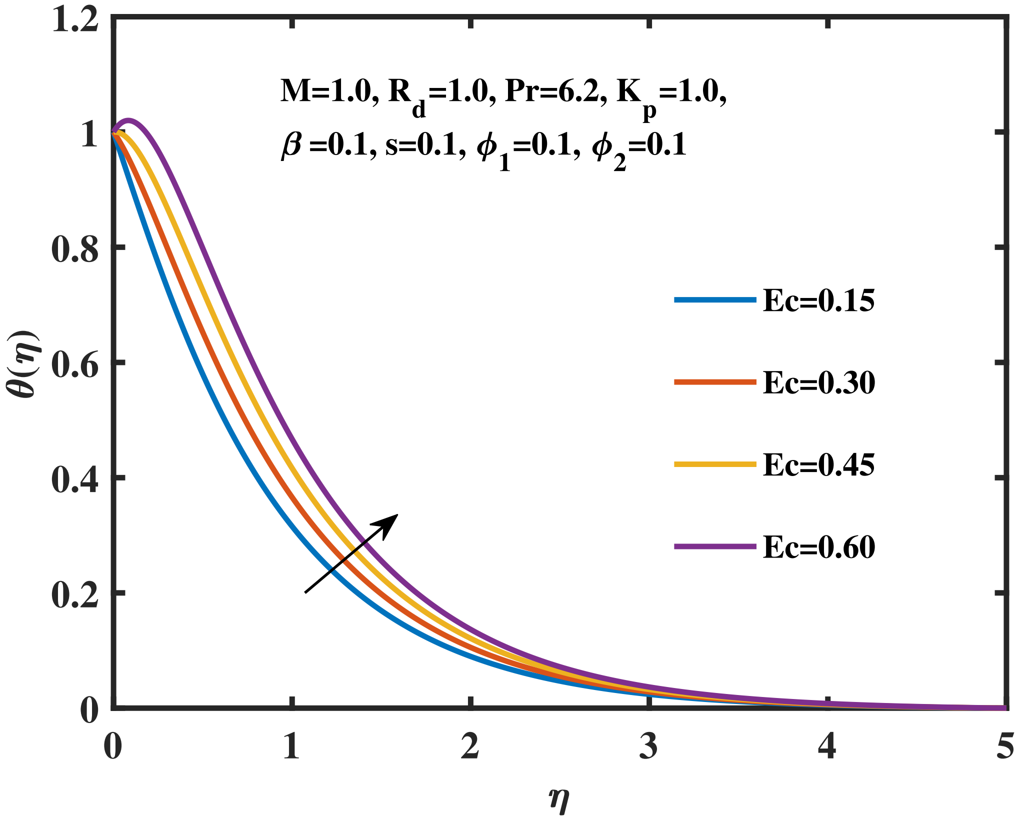

Figure 7. Variation of the temperature $\theta(\eta)$ with η for several values of the Eckert number Ec.

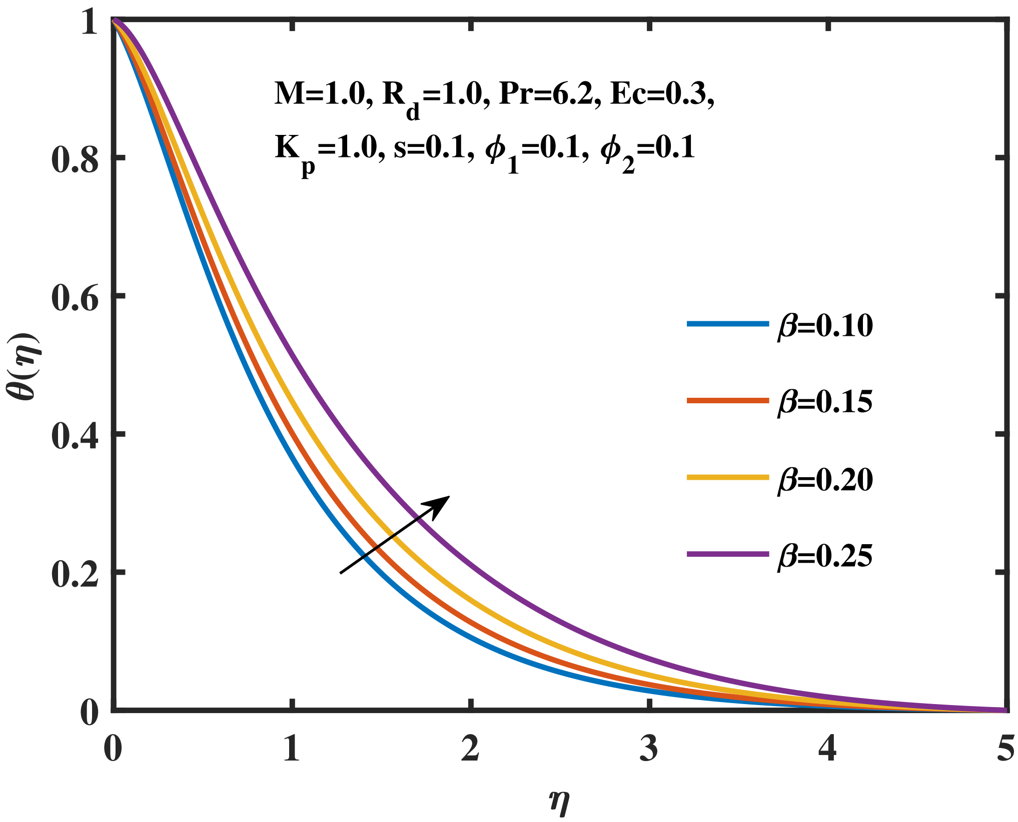

Figure 8. Variation of the temperature $\theta(\eta)$ with η for several values of the heat source parameter β.

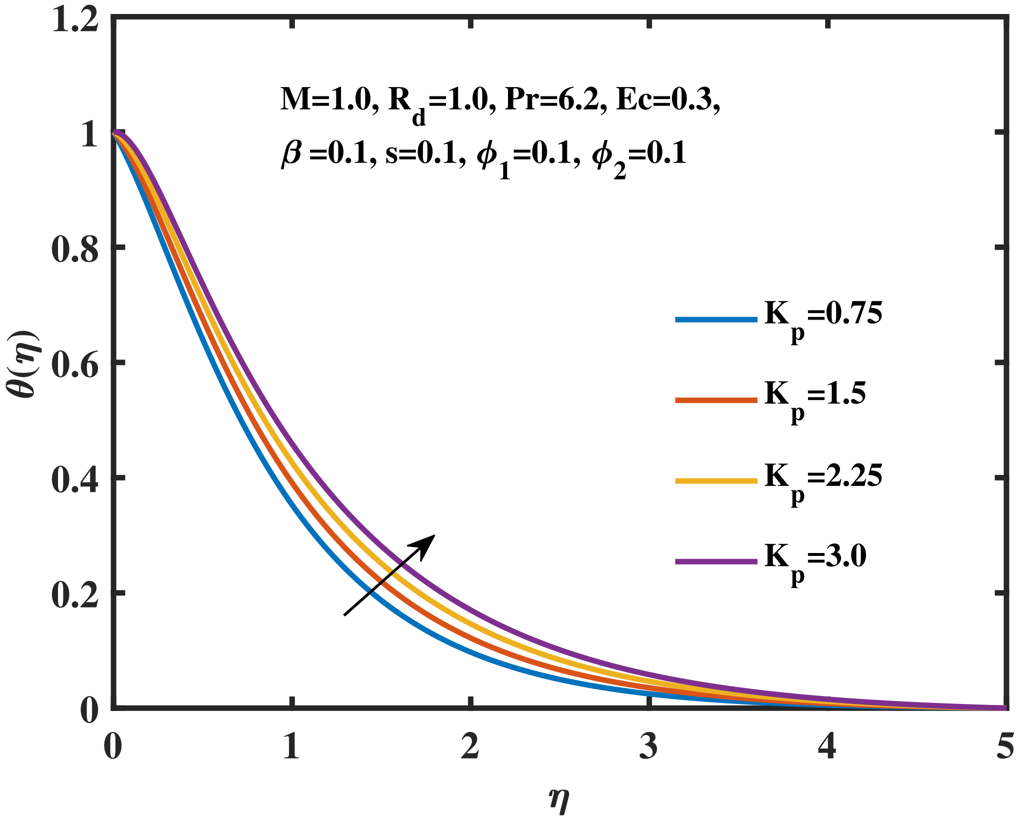

Figure 9. Variation of the temperature $\theta(\eta)$ with η for several values of the porosity parameter K_p.

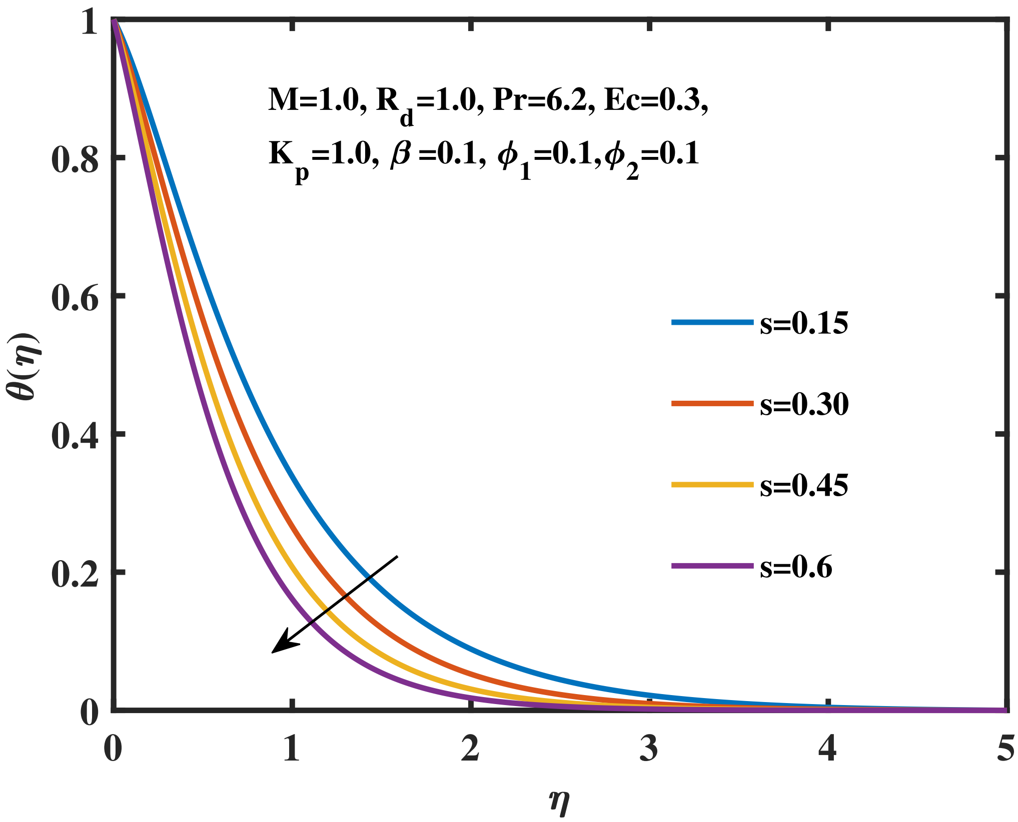

Figure 10. Variation of the temperature $\theta(\eta)$ with η for several values of the suction parameter s.

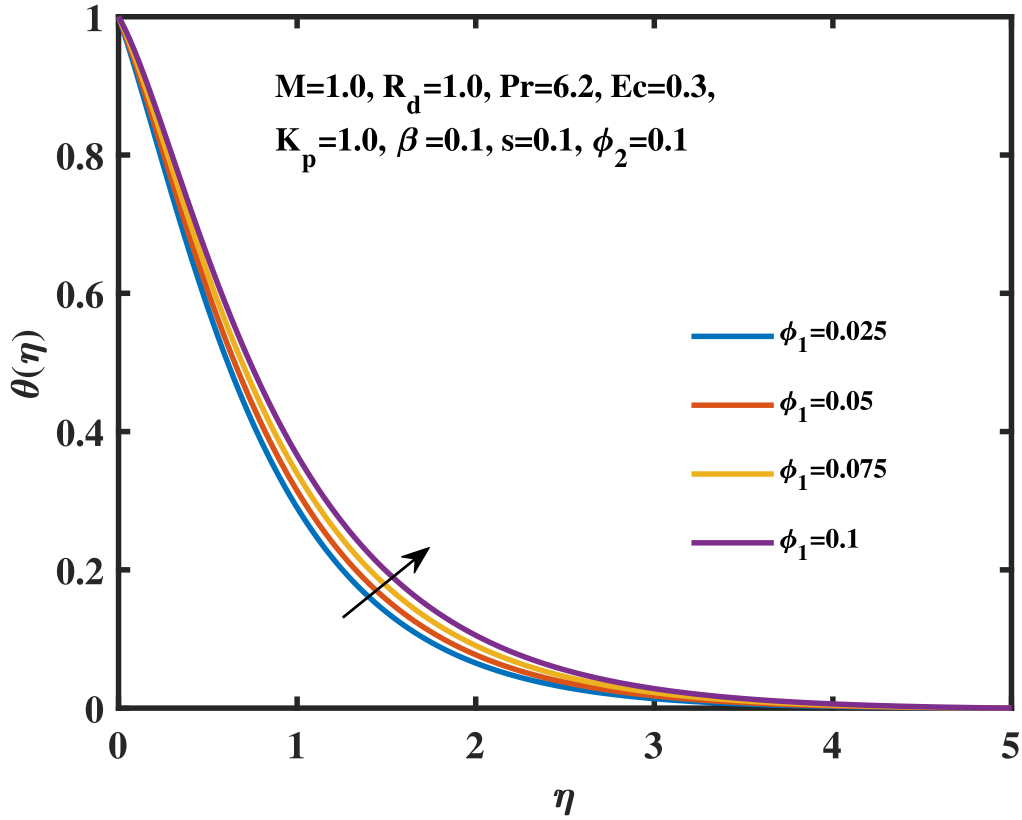

Figure 11. Variation of the temperature $\theta(\eta)$ with η for several values of the volume fraction ϕ_1.

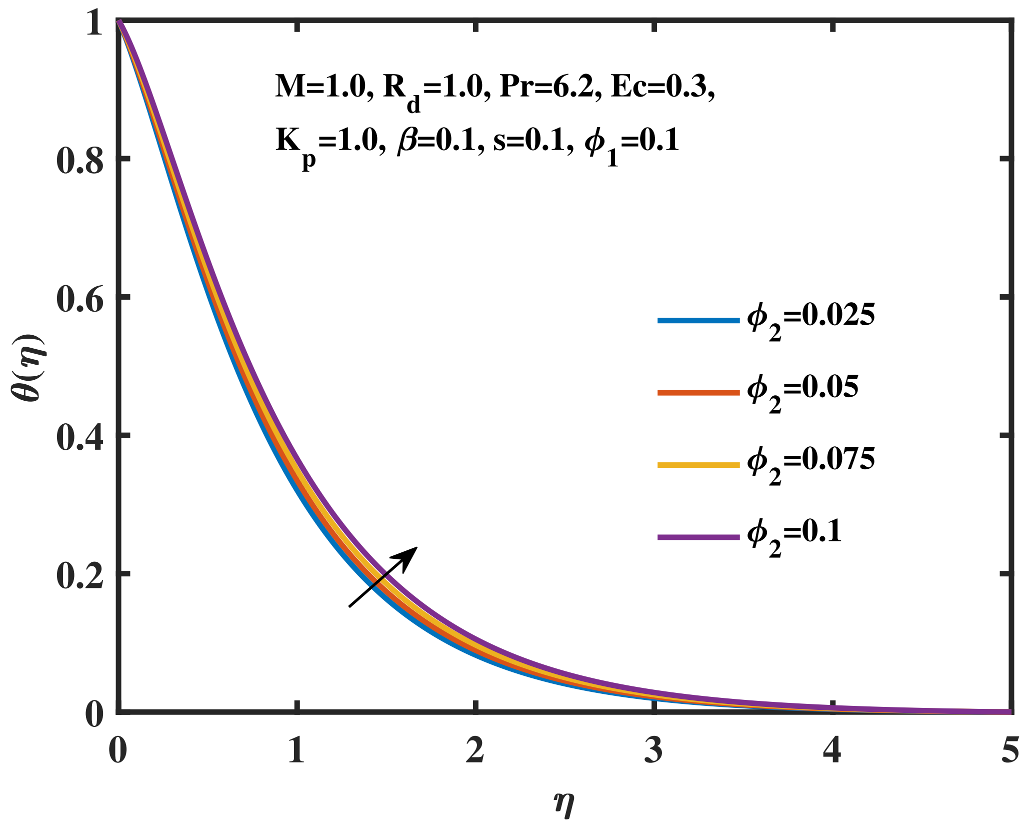

Figure 12. Variation of the temperature $\theta(\eta)$ with η for several values of the volume fraction ϕ_2.

6. Conclusions

In the paper, we have comprehensively examined the effects of hybrid nanoparticles on the fluid flow and heat transfer induced by an exponentially stretching sheet. For validation purposes, our numerical outcomes were compared with previously published data, with good agreement being achieved. The influences of the different parameters on fluid profiles were numerically solved using the Runge–Kutta method with shooting technique. Our significant findings are summarized below:

- The velocity profile is adversely affected by the magnetic field, whereas the temperature is positively impacted.
- The velocity profile is lowered by an increase in the porosity parameter, while the temperature is increased.
- The temperature profiles are proportional to the changes in the radiation parameter, magnetic field parameter, Eckert number, and volume fractions of TiO_2 and Ag nanoparticles.
- The magnetic, suction, and porosity parameters are all inversely linked to the drag coefficient, as are the volume fractions of TiO_2 and Ag nanoparticles.
- The radiation parameter has a positive correlation with the heat transfer rate, while the magnetic parameter, heat source parameter, viscous dissipation parameter, and volume fractions of TiO_2 and Ag nanoparticles all have negative correlations.

In future research, the analysis provided in this paper could be expanded by taking into account other non-Newtonian fluids, as well as favorable effects such as nonlinear thermal radiation and space-dependent heat sources.

Author Contributions: Conceptualization, M.Z.; Software, A.B.; Validation, A.B.; Formal analysis, T.U.; Data curation, M.Z.; Writing—original draft, M.Z.; Writing—review & editing, A.B., T.U. and B.A.; Visualization, A.B., T.U. and B.A.; Supervision, B.A. and G.L.; Funding acquisition, G.L. All authors have read and agreed to the published version of the manuscript.

Funding: This research received no external funding.

Data Availability Statement: Not applicable

Acknowledgments: The authors would like to thank the Lodz University of Technology for offering computing resources for this research.

Conflicts of Interest: The authors declare that they have no known competing financial interest or personal relationships that could have influenced or appeared to influence the work reported in this paper.

References

1. Choi, S.U.; Eastman, J.A. *Enhancing Thermal Conductivity of Fluids with Nanoparticles*; Technical Report; Argonne National Lab: Argonne, IL, USA, 1995.
2. Khan, W.; Pop, I. Boundary-layer flow of a nanofluid past a stretching sheet. *Int. J. Heat Mass Transf.* **2010**, *53*, 2477–2483. [CrossRef]
3. Hayat, T.; Khan, M.I.; Qayyum, S.; Alsaedi, A. Entropy generation in flow with silver and copper nanoparticles. *Colloids Surfaces A Physicochem. Eng. Asp.* **2018**, *539*, 335–346. [CrossRef]
4. Hsiao, K.L. Micropolar nanofluid flow with MHD and viscous dissipation effects towards a stretching sheet with multimedia feature. *Int. J. Heat Mass Transf.* **2017**, *112*, 983–990. [CrossRef]
5. Akbar, N.S.; Nadeem, S.; Haq, R.U.; Khan, Z. Radiation effects on MHD stagnation point flow of nano fluid towards a stretching surface with convective boundary condition. *Chin. J. Aeronaut.* **2013**, *26*, 1389–1397. [CrossRef]
6. Mustafa, I.; Javed, T.; Ghaffari, A. Heat transfer in MHD stagnation point flow of a ferrofluid over a stretchable rotating disk. *J. Mol. Liq.* **2016**, *219*, 526–532. [CrossRef]
7. Ibrahim, W.; Shankar, B.; Nandeppanavar, M.M. MHD stagnation point flow and heat transfer due to nanofluid towards a stretching sheet. *Int. J. Heat Mass Transf.* **2013**, *56*, 1–9. [CrossRef]
8. Mathews, J.; Hymavathi, T. Magnetohydrodynamic stagnation point flow and heat transfer effects of Al_2O_3-Cu/water hybrid nanofluid over a porous stretching surface. *Proc. Inst. Mech. Eng. Part E J. Process. Mech. Eng.* **2023**, *237*, 1064–1072. [CrossRef]
9. Javed, T.; Ghaffari, A.; Ahmad, H. Numerical study of unsteady MHD oblique stagnation point flow with heat transfer over an oscillating flat plate. *Can. J. Phys.* **2015**, *93*, 1138–1143. [CrossRef]

10. Sarkar, J.; Ghosh, P.; Adil, A. A review on hybrid nanofluids: Recent research, development and applications. *Renew. Sustain. Energy Rev.* **2015**, *43*, 164–177. [CrossRef]
11. Devi, S.S.U.; Devi, S.A. Numerical investigation of three-dimensional hybrid Cu-Al_2O_3/water nanofluid flow over a stretching sheet with effecting Lorentz force subject to Newtonian heating. *Can. J. Phys.* **2016**, *94*, 490–496. [CrossRef]
12. Khashi'ie, N.S.; Arifin, N.M.; Nazar, R.; Hafidzuddin, E.H.; Wahi, N.; Pop, I. Magnetohydrodynamics (MHD) axisymmetric flow and heat transfer of a hybrid nanofluid past a radially permeable stretching/shrinking sheet with Joule heating. *Chin. J. Phys.* **2020**, *64*, 251–263. [CrossRef]
13. Leong, K.Y.; Razali, I.; Ahmad, K.K.; Ong, H.C.; Ghazali, M.J.; Rahman, M.R.A. Thermal conductivity of an ethylene glycol/water-based nanofluid with copper-titanium dioxide nanoparticles: An experimental approach. *Int. Commun. Heat Mass Transf.* **2018**, *90*, 23–28. [CrossRef]
14. Gul, T.; Saeed, A. Nonlinear mixed convection couple stress tri-hybrid nanofluids flow in a Darcy–Forchheimer porous medium over a nonlinear stretching surface. *Waves Random Complex Media* **2022**, 1–18. [CrossRef]
15. Basit, A.; Asjad, M.I.; Akgül, A. Convective flow of a fractional second grade fluid containing different nanoparticles with Prabhakar fractional derivative subject to non-uniform velocity at the boundary. *Math. Methods Appl. Sci.* **2023**, *46*, 8148–8159. [CrossRef]
16. Mahabaleshwar, U.; Anusha, T.; Hatami, M. The MHD Newtonian hybrid nanofluid flow and mass transfer analysis due to super-linear stretching sheet embedded in porous medium. *Sci. Rep.* **2021**, *11*, 22518. [CrossRef] [PubMed]
17. Kayalvizhi, J.; Vijaya Kumar, A. Entropy Analysis of EMHD Hybrid Nanofluid Stagnation Point Flow over a Porous Stretching Sheet with Melting Heat Transfer in the Presence of Thermal Radiation. *Energies* **2022**, *15*, 8317. [CrossRef]
18. Waqas, H.; Farooq, U.; Liu, D.; Abid, M.; Imran, M.; Muhammad, T. Heat transfer analysis of hybrid nanofluid flow with thermal radiation through a stretching sheet: A comparative study. *Int. Commun. Heat Mass Transf.* **2022**, *138*, 106303. [CrossRef]
19. Crane, L.J. Flow past a stretching plate. *Z. Angew. Math. Phys. ZAMP* **1970**, *21*, 645–647. [CrossRef]
20. Magyari, E.; Keller, B. Heat and mass transfer in the boundary layers on an exponentially stretching continuous surface. *J. Phys. D Appl. Phys.* **1999**, *32*, 577. [CrossRef]
21. Hayat, T.; Khan, M.I.; Waqas, M.; Alsaedi, A.; Farooq, M. Numerical simulation for melting heat transfer and radiation effects in stagnation point flow of carbon–water nanofluid. *Comput. Methods Appl. Mech. Eng.* **2017**, *315*, 1011–1024. [CrossRef]
22. Mabood, F.; Khan, W.; Ismail, A.M. MHD flow over exponential radiating stretching sheet using homotopy analysis method. *J. King Saud Univ.-Eng. Sci.* **2017**, *29*, 68–74. [CrossRef]
23. Zaib, A.; Bhattacharyya, K.; Shafie, S. Unsteady boundary layer flow and heat transfer over an exponentially shrinking sheet with suction in a copper-water nanofluid. *J. Cent. South Univ.* **2015**, *22*, 4856–4863. [CrossRef]
24. Abd El-Aziz, M. Viscous dissipation effect on mixed convection flow of a micropolar fluid over an exponentially stretching sheet. *Can. J. Phys.* **2009**, *87*, 359–368. [CrossRef]
25. Dessie, H.; Kishan, N. MHD effects on heat transfer over stretching sheet embedded in porous medium with variable viscosity, viscous dissipation and heat source/sink. *Ain Shams Eng. J.* **2014**, *5*, 967–977. [CrossRef]
26. Cortell, R. Effects of viscous dissipation and radiation on the thermal boundary layer over a nonlinearly stretching sheet. *Phys. Lett. A* **2008**, *372*, 631–636. [CrossRef]
27. Rafique, K.; Mahmood, Z.; Alqahtani, H.; Eldin, S.M. Various nanoparticle shapes and quadratic velocity impacts on entropy generation and MHD flow over a stretching sheet with joule heating. *Alex. Eng. J.* **2023**, *71*, 147–159. [CrossRef]
28. Alharbi, K.A.M.; Farooq, U.; Waqas, H.; Imran, M.; Noreen, S.; Akgül, A.; Baleanu, D.; El Din, S.M.; Abbas, K. Numerical solution of Maxwell-Sutterby nanofluid flow inside a stretching sheet with thermal radiation, exponential heat source/sink, and bioconvection. *Int. J. Thermofluids* **2023**, *18*, 100339. [CrossRef]
29. Yirga, Y.; Tesfay, D. Heat and mass transfer in MHD flow of nanofluids through a porous media due to a permeable stretching sheet with viscous dissipation and chemical reaction effects. *Int. J. Mech. Aerosp. Ind. Mechatron. Manuf. Eng.* **2015**, *9*, 1–8.
30. Hayat, T.; Abbas, Z.; Javed, T. Mixed convection flow of a micropolar fluid over a non-linearly stretching sheet. *Phys. Lett. A* **2008**, *372*, 637–647. [CrossRef]
31. Haroun, N.A.; Mondal, S.; Sibanda, P. Hydromagnetic nanofluids flow through a porous medium with thermal radiation, chemical reaction and viscous dissipation using the spectral relaxation method. *Int. J. Comput. Methods* **2019**, *16*, 1840020. [CrossRef]
32. Acharya, N.; Das, K.; Kumar Kundu, P. Ramification of variable thickness on MHD TiO_2 and Ag nanofluid flow over a slendering stretching sheet using NDM. *Eur. Phys. J. Plus* **2016**, *131*, 303. [CrossRef]
33. Goud, B.S.; Srilatha, P.; Bindu, P.; Krishna, Y.H. Radiation effect on MHD boundary layer flow due to an exponentially stretching sheet. *Adv. Math. Sci. J.* **2020**, *9*, 10755–10761. [CrossRef]
34. Waini, I.; Ishak, A.; Pop, I. Hybrid nanofluid flow induced by an exponentially shrinking sheet. *Chin. J. Phys.* **2020**, *68*, 468–482. [CrossRef]
35. Rosseland, S. *Astrophysics and Atomic Theoretical Foundations*; Springer: Berlin/Heidelberg, Germany, 1931.
36. Ishak, A. MHD boundary layer flow due to an exponentially stretching sheet with radiation effect. *Sains Malays.* **2011**, *40*, 391–395.
37. Bhattacharyya, K. Boundary layer flow and heat transfer over an exponentially shrinking sheet. *Chin. Phys. Lett.* **2011**, *28*, 074701. [CrossRef]

38. Bidin, B.; Nazar, R. Numerical solution of the boundary layer flow over an exponentially stretching sheet with thermal radiation. *Eur. J. Sci. Res.* **2009**, *33*, 710–717.
39. Versaci, M.; Jannelli, A.; Angiulli, G. Electrostatic micro-electro-mechanical-systems (MEMS) devices: A comparison among numerical techniques for recovering the membrane profile. *IEEE Access* **2020**, *8*, 125874–125886. [CrossRef]
40. Mandal, I.C.; Mukhopadhyay, S. Heat transfer analysis for fluid flow over an exponentially stretching porous sheet with surface heat flux in porous medium. *Ain Shams Eng. J.* **2013**, *4*, 103–110. [CrossRef]
41. Naramgari, S.; Sulochana, C. Dual solutions of radiative MHD nanofluid flow over an exponentially stretching sheet with heat generation/absorption. *Appl. Nanosci.* **2016**, *6*, 131–139. [CrossRef]